Science Bulletin 64 (2019) 1067–1079

Contents lists available at ScienceDirect

Science Bulletin

journal homepage: www.elsevier.com/locate/scib

Science Bulletin
www.scibull.com

Review

Black phosphorus electronics

Hao Huang [a], Bei Jiang [a], Xuming Zou [b,*], Xingzhong Zhao [b,*], Lei Liao [a,b,*]

[a] School of Physics and Technology, Wuhan University, Wuhan 430072, China
[b] Key Laboratory for Micro/Nano-Optoelectronic Devices of Ministry of Education, School of Physics and Electronics, Hunan University, Changsha 410082, China

ARTICLE INFO

Article history:
Received 4 December 2018
Received in revised form 23 January 2019
Accepted 12 February 2019
Available online 23 February 2019

Keywords:
Anisotropy
Doping
Superlattices
Contact
Dielectric
Transistors

ABSTRACT

As the scaling of silicon-based field-effect transistors has approached its physical limits, the search for alternative channel materials for future logic devices has attracted much attention. The discovery of graphene has unveiled another material family with layered structures called two-dimensional (2D) materials. Black phosphorus (BP), the most stable allotrope of phosphorus, was introduced as a new type of 2D material in 2014. Thanks to its high mobility, in-plane anisotropy and direct band gap, BP is considered to be a promising candidate for next-generation electronic and optoelectronic devices. Numerous studies have demonstrated the beneficial effects of introducing BP for device architectures. Herein, we present a review outlining recent progress towards high performance BP-based transistors. This review starts with the fundamental properties of BP, including its crystal structure, bandgap, and direct current (DC) and radio-frequency (RF) characteristics, followed by a detailed description of the modulation and application of those properties, involving anisotropy, functionalization and superlattices. Furthermore, we also discuss device design for high-performance transistors, with particular emphasis on interface engineering and device stability. Finally, we offer our perspective on the future of BP electronics, aiming to benefit colleagues who are interested in this exciting research field.

1. Introduction

Moore's law, the principle that has powered the information-technology revolution since the 1960s, is nearing its end [1]. Currently, silicon, which has been the most suitable material for field-effect transistors (FETs) for decades, is rapidly approaching its ultimate physical limits that arise from short channel effects [2]. In addtion, the loss of electrostatic gate control on the channel and direct source-to-drain tunneling make it difficult to further scale down Si FETs [3]. A single layer of carbon atoms with a honeycomb lattice, which is called graphene, has attracted great attention towards two dimensional (2D) materials since it was discovered in 2004 [4]. To date, numerous 2D materials have been reported, covering a range of categories from insulators to metals such as hexagonal boron nitride (h-BN) [5,6], transition metal dichalcogenides (TMDs) [7], and black phosphorus (BP) [8]. Unlike conventional bulk materials, 2D semiconductor materials are immune to short channel effects due to their atomic thickness, which offers the opportunity for ultimate scaling beyond the 5 nm gate length. With the exploration of 2D materials for electronics, graphene has proved to be unsuitable for logic circuits due to its zero energy bandgap. Although TMDs such as molybdenum sulfide (MoS_2) have satisfactory bandgap, their carrier mobilities are relatively low, resulting in limited performance for high speed integrated circuits. In comparison, BP, which has superior carrier mobility (~1,000 cm^2 /(V s)) and a tunable direct bandgap (from 0.3 to 1.2 eV), is regarded as a bridge between MoS_2 and graphene so that it may be widely used in future electronics.

BP, the most stable allotrope of phosphorus, was discovered during an attempt to produce red phosphorus by Bridgman in 1914 [9]. However, BP did not attract much attention throughout the century after its discovery until the first few-layer BP field-effect transistor was successfully fabricated in 2014 [8]. To date, thousands of articles about BP have been published within 4 years, both in theory and in experiment, covering the range from synthesis to applications [10–15]. In this review, we focus on BP electronics. First, the fundamental properties of BP are introduced and then we provide a detailed description of the modulation and application of those properties, involving anisotropy, functionalization, and superlattices. Moving forward, device design for high-performance transistors is also discussed, with particular emphasis on interface engineering and device stability. Finally, we summarize the current status of BP electronics and look forward to the continued development of black

SPECIAL TOPIC: Two-dimensional Materials: New Opportunities for Electronics, Photonics and Optoelectronics

* Corresponding authors.
E-mail addresses: zouxuming@hnu.edu.cn (X. Zou), 00006796@whu.edu.cn (X. Zhao), liaolei@whu.edu.cn (L. Liao).

https://doi.org/10.1016/j.scib.2019.02.015
2095-9273/

phosphorus electronics, aiming to benefit colleagues who are interested in this exciting research field.

2. Fundamental properties

2.1. Crystal structure and bandgap

Fig. 1a demonstrates the crystal structure of few-layer BP [8]. Similar to graphene, bulk BP consists of repeating single layers bound together by van der Waals (vdW) interactions so that single- or few-layers BP can be esaily obtained by mechanical exfoliation. The thickness of monolayer BP (phosphorene) has been determined to be ~ 5 Å. However, in the BP lattice, each phosphorus atom is covalently bonded with three adjacent phosphorus atoms to form two inequivalent directions, so phosphorene is generally considered to be composed of two atomic layers. Otherwise, the directions parallel and perpendicular to the atomic ridges correspond to the armchair and zigzag directions, respectively. Hence, anisotropy can be clearly observed in BP crystals, offering more possibilities for the design and fabrication of novel devices. The bandgap of BP varies with the number of layers; this has been demonstrated both in theory [16] and in experiment [17] as shown in Fig. 1b. Obviously, the bandgap of BP increases monotonically as the layer thickness decreases. A power law can be employed to describe this dependency, while the power exponent usually relates to the quantum confinement effect. Normally, the power exponent that perfectly matches this quantum confinement effect is 2. However, the power exponent of BP is usually far less than this value, so the variation of the bandgap cannot be explained with the conventional model. Tran et al. [16] explained that this weaker quantum confinement effect may be caused by the vdW interfaces, which partially isolate electrons between neighboring sheets. Fig. 1c exhibits the extracted energy bands of BP. Black dots and red dots represent the conduction and valence bands of BP films with different numbers of layers, respectively. What is more, dark yellow dots stand for the Fermi level of BP films of different layers [18]. Notably, with increasing thickness, the Fermi level moves closer to the valence band, resulting in p-type characteristics which are usually obvious in BP-based devices. It is important to note that the band gap of BP covers the range of 0.3-1.2 eV (based on calculated theoretical values close to experimental data), which can bridge the energy gap between the zero band gap of graphene and the relatively large band gap of TMDs. Fig. 2 demonstrates carrier mobilities versus current on/off ratio reported for field-effect transistors based on typical 2D materials including graphene

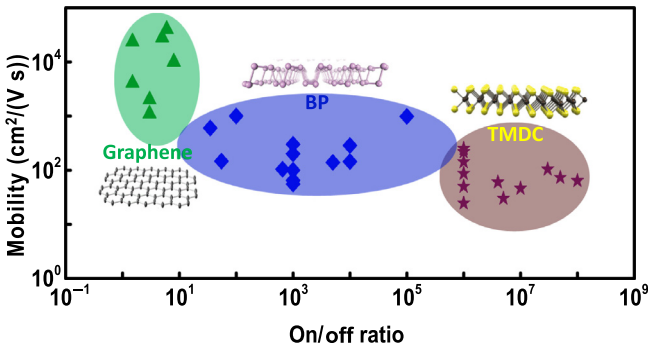

Fig. 2. Carrier mobility versus current on/off ratio reported for typical 2D materials electronics.

[4,19–24], TMDs [7,25–32] and BP [8,25,33–39]. As shown in Fig. 2, transistors that are bases on different 2D materials fall into different zones due to the different band gaps, and these zones correspond to several key application domains in electronics. The application of BP can fill the gap between graphene and TMDs to enable the application of 2D materials under various conditions.

2.2. First few-layer BP transistors

The first few-layer BP FETs were successfully fabricated by Li et al. [8]. The thin flakes of BP were mechanically exfoliated and transferred onto doped silicon wafers covered with a layer of thermally grown silicon dioxide. Cr and Au (typically 5 and 60 nm, respectively) were then deposited on the BP as metal contacts. A schematic of the device structure of a few-layer phosphorene FET is demonstrated in Fig. 3a. The results obtained from a device with a 5-nm-thick channel on top of a 90 nm SiO_2 gate dielectric are shown in Fig. 3b. Red and green curves correspond to V_{ds} = 10 and 100 mV, respectively. An on/off ratio of ~10^5, subthreshold swing (SS) of ~4.6 V/decade, and mobility of ~55 $cm^2/(V\,s)$ could be obtained. Moreover, a highest mobility of ~ 984 $cm^2/(V\,s)$ could be observed when the thickness was increased to 10 nm. Fig. 3c shows the temperature dependence of the mobility (both field effect mobility and Hall mobility) of an 8 nm thick BP channel FET. Both values showed a similar temperature dependence decreasing mobility at temperatures higher than 100 K and saturation (or slight decrease for low carrier densities) at lower temper-

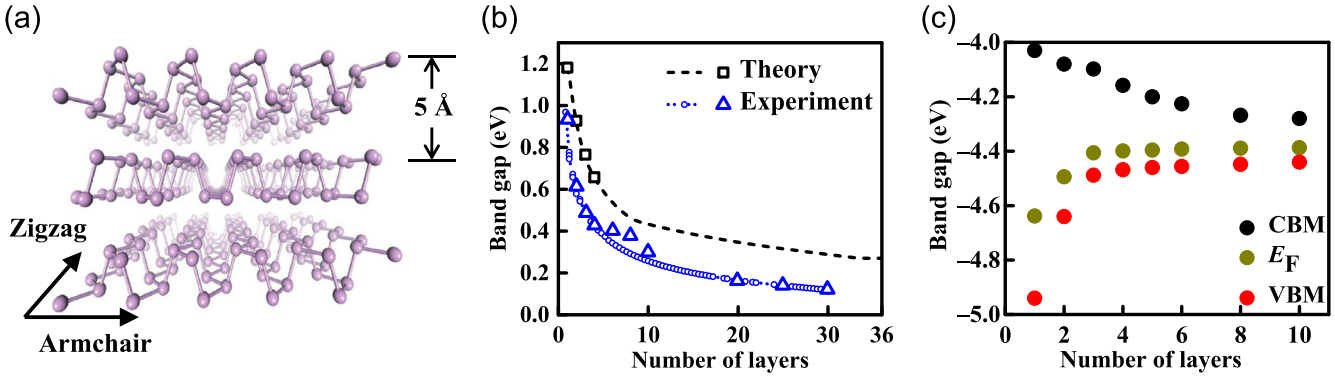

Fig. 1. The crystal structure and bandgap of BP. (a) The schematic diagram of the crystal structure of BP. Reprinted with permission from Ref. [8]. Copyright © 2014, Springer Nature. (b) Thickness depend band gap of BP, both in theory and in experiment. Reprinted with permission from Ref. [16,17]. Copyright © 2014, American Physical Society. Copyright © 2014, American Chemical Society. (c) The extracted energy bands of BP, Black dots and red dots are conduction and valence bands of different layers BP. Dark yellow dots are Fermi level of different layers BP. Reprinted with permission from Ref. [18]. Copyright © 2018, John Wiley and Sons.

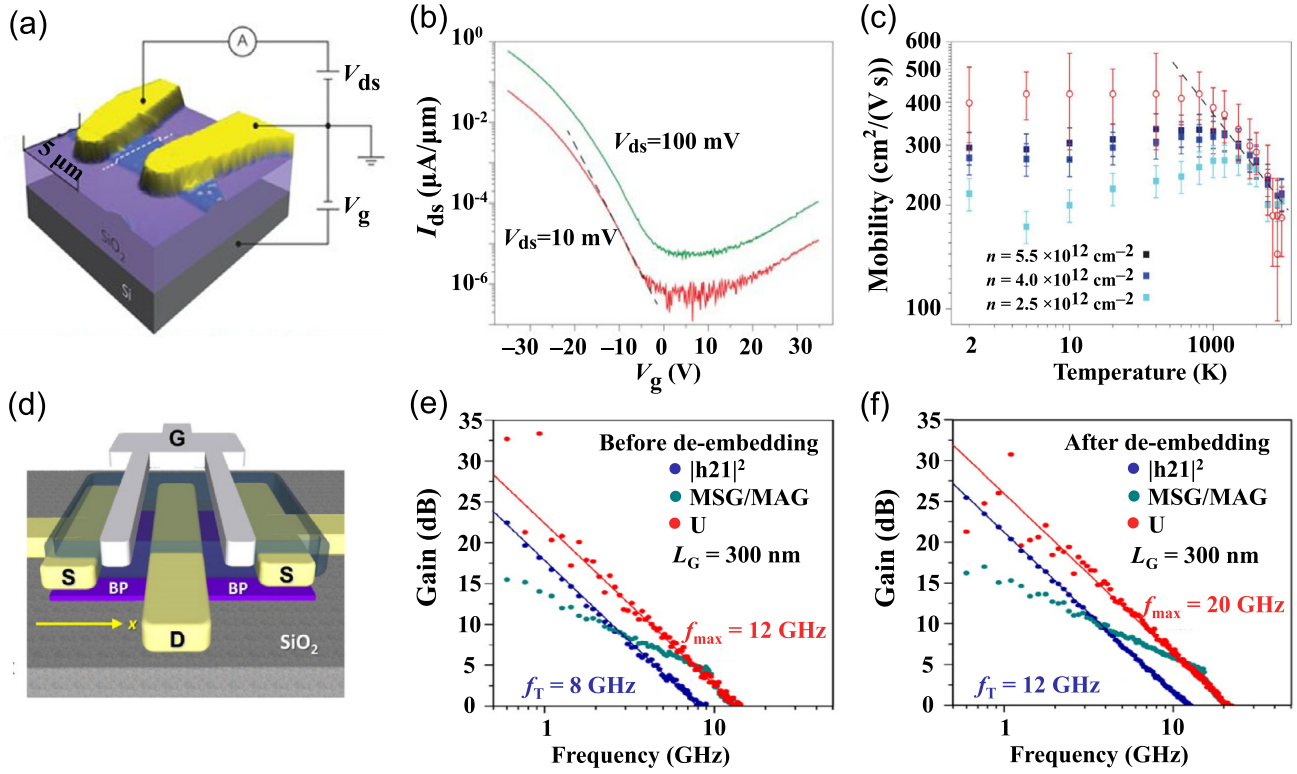

Fig. 3. The DC and RF characteristic of few layer BP transistors. (a) Schematic of device structure of a few-layer BP FET. (b) Transfer characteristics at V_{ds} = 10 and 100 mV. (c) Field effect mobility (open circles) and Hall mobility (filled squares, three different values of carrier density (n)) as a function of temperature on a logarithmic scale. Reprinted with permission from Ref. [8]. Copyright © 2014, Springer Nature. (d) Schematic of the BP RF transistor device structure. (e, f) The short-circuit current gain h21, MSG/MAG, and unilateral power gain U of the 300 nm channel length device before (e) and after (f) de-embedding. Reprinted with permission from Ref. [40]. Copyright © 2014, American Chemical Society.

atures. This can be explained by conventional high-temperature phonon-scatting and low-temperature impurities-scatting models. This work proved the potential for BP applications in the field of electronics, and since then, a number of efforts have been made to implement a wide range of high-performance electronics based on BP.

2.3. BP radio-frequency transistors

The first BP RF transistors were demonstrated by Wang et.al. [40]. A schematic of the BP transistor structure is shown in Fig. 3d. In this transistor, an 8.5 nm BP flake and an 21 nm hafnium oxide (HfO_2) layer were employed as channel and gate oxide, respectively. Fig. 3b and c plots the short-circuit current gain (h21), unilateral power gain (U), and maximum stable gain (MSG)/maximum available gain (MAG) before and after de-embedding measured at V_{ds} = −2.0 V and V_{gs} = −1.7 V, respectively. It is well known that the short-circuit current gain cut-off frequency (f_T) and maximum oscillation frequency (f_{max}) are the most important figures-of-merit to evaluate the high frequency performance of transistors, as f_T is related to the intrinsic speed and f_{max} represent the highest possible operating frequency [40]. In this work, the device was found to have f_T = 7.8 GHz and f_{max} = 12 GHz before de-embedding and f_T = 12 GHz and f_{max} = 20 GHz after de-embedding, indicating that BP transistors can operate in the gigahertz frequency range. In addition, intrinsic $f_T \sim 17.5$ GHz and $f_{max} \sim 14.5$ GHz were also obtained from flexible top-gated (TG) BP transistors in subsequent work [41]. More importantly, in theory, both the intrinsic f_T and f_{max} of BP transistors exceeded 10 THz [42,43]. While intrinsic f_T increases monotonically with channel length scaling, f_{max} starts to degrade when the channel length becomes less than 30 nm. Hence, the results obtained from previous works prove that BP is a promising candidate for future electronics technology for operation in the multi-GHz and THz frequency range in both conventional and flexible electronics.

3. Tunable materials properties

In addition to clarifying the fundamental properties of BP, the modulation or reconstruction of those properties in a direction that is beneficial to us is particularly important. Numerous efforts have been made to achieve this goal. In this chapter, some interesting properties of BP will be introduced in detail, and several effective means of regulating these properties will also be discussed.

3.1. Layer and anisotropy

Controlling the thickness of the flake is the simplest and most effective way to control the properties of BP-based electronics. Fig. 4a shows the transfer characteristic curves of FETs fabricated with different BP thicknesses, which were measured with a source-drain voltage (V_{ds}) of −1 V at room temperature [18]. It is obvious from the figure that the off-current (I_{off}) and the on-current (I_{on}) of the FETs are strongly dependent on BP thickness; that is, both of values increase monotonically with increasing BP thickness. The increase in I_{off} can be explained by the reduced of band gap and Schottky barrier height (SBH) which come with decreased BP body thickness due to the fact that the I_{off} is mainly dominated by the thermionic emission model. It is worth noting that the increase in I_{off} is more intense than the increase in I_{on}, leading to a reduced current on/off ratio (I_{on}/I_{off}) and deteriorating device performance. Thus, a suitable thickness should be chosen to realize the best balance between I_{on} and on/off ratio. One of the most critical parameters for characterizing device performance is

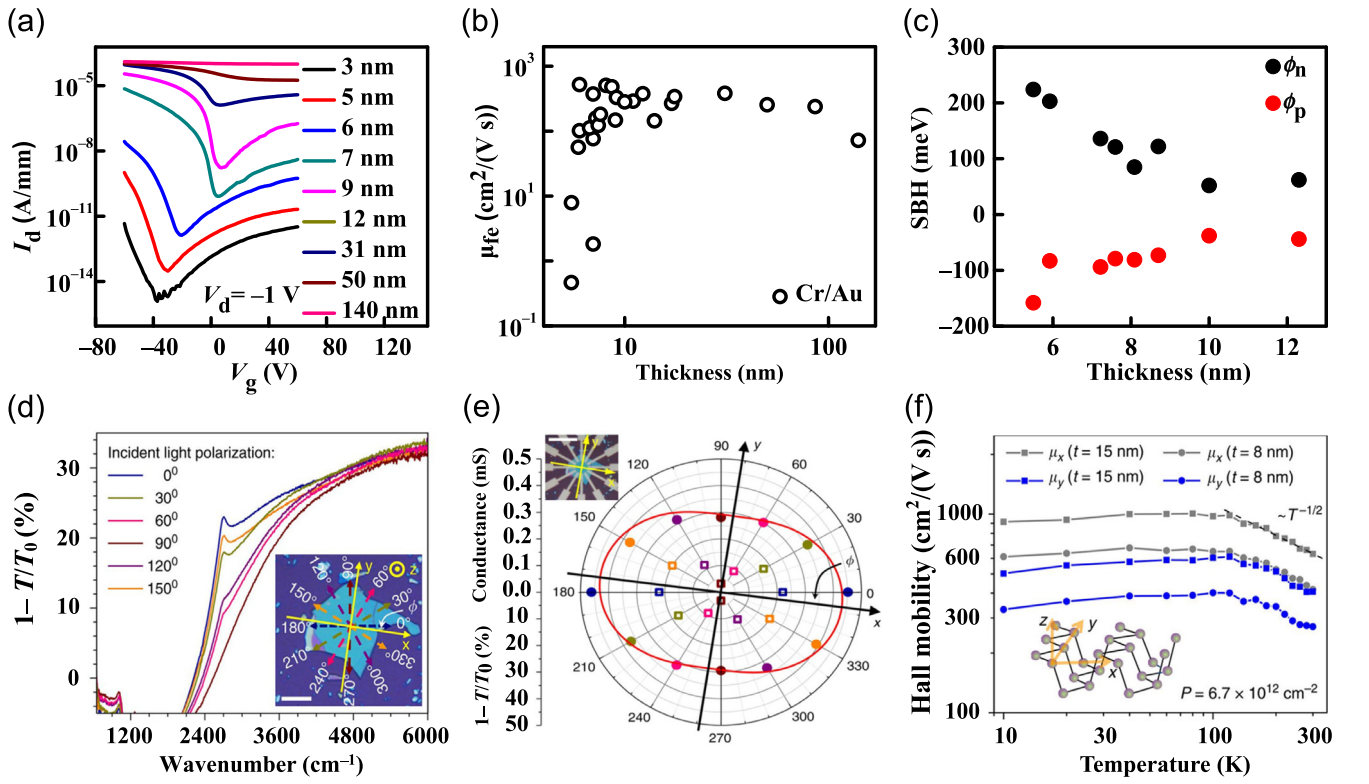

Fig. 4. (Color online) The layer-dependent and anisotropy properties of BP transistors. (a) The transfer characteristics of BP FETs with different thickness. (b) The extracted field effect mobility values of BP FETs. (c) The experimentally extracted SBH for different thickness BP FETs. The dots are n-type and p-type SBH, respectively. Reprinted with permission from Ref. [18]. Copyright © 2018, John Wiley and Sons. (d) Polarization-resolved infrared relative extinction spectra when light is polarized along the six directions as shown in the inset. Inset: an optical micrograph of a BP flake with a thickness of around 30 nm. Scale bar: 20 mm. (e) DC conductivity and IR relative extinction measured along the same six directions on this BP flake and plotted in polar coordinates. The angle-resolved DC conductance (solid dots) and the polarization-resolved relative extinction of the same flake at 2,700 cm^{-1} (hollow squares) are shown on the same polar plot. Dots and squares of the same color correspond to the directions indicated by the arrows in the inset in (d). Inset: an optical image of this BP flake with 12 electrodes spaced at 30° apart. Scale bar: 50 mm. (f) Hall mobility measured at a constant hole doping concentration of 6.7 × 10^{12} cm^{-2} along the x (m_x) and y (m_y) directions for BP thin films with a thickness of 8 and 15 nm, respectively. Reprinted with permission from Ref. [44]. Copyright © 2014, Springer Nature.

the field effect mobility, and the extracted field effect mobility values of BP FETs with different thickness are displayed in Fig. 4b. The relationship between mobility and layer thickness can be divided into three parts, below ~5 , 5–10, and above ~10 nm. First, in the region below ~5 nm, the mobility sharply increases with increasing BP thickness and corresponds to the Schottky-Mott rule. Second, for BP thicknesses between ~ 5 and 10 nm, the mobility seems to vary only slightly because the Fermi energy pinning effect dominates the contact resistance. Lastly, when the thickness of BP exceeds ~10 nm, the trend of decresing mobility with increasing layer thickness begin to appear; that is, the interlayer resistance becomes a critical factor in current transport and limits the current flow in the top layers [45]. To further reveal the variation of SBH with BP thickness, the experimentally extracted SBH for different thickness BP FETs are presented in Fig. 4c. Evidently, the SBH of thin BP flakes is significantly higher than that of a thick one, in agreement with previous electrical analysis by the same measure, and similar results have also been obtained in theoretical calculations [17,38]. Through a systematic study of the thickness-related properties, high-performance electronic devices can be achieved by adjusting the layer thickness, which lays a solid foundation for the future development of BP electronics.

Besides, anisotropy is the biggest advantage of BP compared to other typical two-dimensional materials, since its unique properties generate opportunities for fabricating conceptually novel devices and applications. This anisotropy was reported in an early study of bulk BP [46]. By calculating the effective mass of electron holes in different directions, anisotropy of BP could be analyzed. Notably, there is a special phenomenon that the mobility is not positively related to the effective mass. The z-direction has the lowest mobility with an intermediate effective mass, which is most probably caused by the interlayer vdW gap [15]. The anisotropy of BP can also be studied more intuitively using other techniques [44]. Polarization-resolved infrared spectroscopy has been used to investigate the anisotropy of BP, as shown in Fig. 4d. The polarization resolved relative extinction spectrum is represented by the author as $(1 - T/T_0)$, where T is the optical transmission through the BP and the substrate, while T_0 is optical transmission through the substrate only. The value of $(1 - T/T_0)$ was measured as a function of light along the z-direction, and the direction of measurement is indicated by the six colored arrows in the inset of Fig. 4d. A dramatic increase can be observed at around 2,400 cm^{-1}, which indicates that the bandgap is ~0.3 eV and agrees strongly with the previously reported value at the z symmetry point [46]. The corresponding x and y directions were further determined by angle-resolved DC conductance measurements. The structure of the BP device is shown in the inset of Fig. 4e. Apparently, 12 electrodes were fabricated on the same flake separated by 30°. Fig. 4e displays the results of applying an electric field across each pair of diagonally positioned electrodes in polar coordinates, where the ratio of mobility in the x and y direction is 1.5. Similar results were also obtained in the measurement of the angular dependence of the drain current and transconductance (G_m) of a BP device with a film thickness of ~10 nm [33].

However, due to the current spreading, mobility anisotropy is severely underestimated by a simple approach. Hence, Hall mea-

surements were introduced to precisely determine its exact value. Standard Hall bars were fabricated and the mobility in the *x* and *y* directions were measured down to 10 K, as shown in Fig. 4f. This measurement was performed under conditions such that the hole carrier density was kept at 6.7×10^{12} cm^{-2}, and the result shows that the peak mobility of a 15 nm sample along the *x* direction was above 1,000 cm^2/(V s) at 120 K while the value of an 8 nm sample was ~600 cm^2/(V s). With accurate Hall measurements, the mobility in the *x* direction was found to be 1.8 times higher than in the *y* direction, which is slightly larger than that obtained from DC measurements. It is worth noting that the mobility of the BP film is much lower than that of the bulk material (peak value of ~50,000 cm^2/(V s) along the *x* direction [46]), and the thicker film has a higher mobility; this phenomenon could be attributed to the impact of the substrate on the scattering of carriers in BP thin films [47]. As a result, preparing a high quality film will further enhance the performance of BP-based electronic devices.

3.2. Functionalization and doping

Functionalization is an effective and controllable approach to tailoring the properties of BP. Functionalization techniques can be roughly divided into two groups: non-covalent [48] and covalent [49]. Schematic diagrams depicting non-covalent and covalent functionalization are displayed in Fig. 5a and b, respectively. Covalent functionalization is the modification of the performance of BP by the formation of covalent bonds between other materials and BP, while non-covalent functionalization uses materials adsorbed on the surface by interactions. The functionalization of BP was first introduced by Ryder et al. [39] in 2016 using aryl diazonium as a reactant. This modification can proceed spontaneously when BP samples are immersed in aryl diazonium salt solutions, resulting in formatin of phosphorus-carbon bonds, as shown in Fig. 5c. Particularly, the rate of this reaction is sensitive to the reduction potential of the aryl diazonium molecule, indicating that the level of modification can be well controlled. The results of different degrees of functionalization have been systematically studied. Firstly, the semiconductor performance of BP is enhanced with low levels of functionalization, which registers as an increase in carrier mobility and on/off ratio. Then, further functionalization can better protect BP from ambient conditions, which was confirmed by atomic force microscopy (AFM). However, the intralayer phosphorus bonding is disrupted when a high level of functionalization is reached, as evidenced by X-ray photoelectron spectroscopy (XPS) and Raman spectra. Soon afterward, the transport properties and electronic structure of covalently functionalized BP were comprehensive investigated using first-principles caculations [49], which revealed that a flat energy band within the bandgap will be generated by the molecular modification. This flat energy band leads to a decrease in the hole mobility of BP. Meanwhile, the authors claim that a polymer-BP composite is a better choice for generating covalent bonds and functionalizing BP because it can maintain both good electron and hole mobility and has enhanced stability in ambient conditions. Recently, aryl iodonium salts were introduced as a new strategy for the covalent functionalization of liquid exfoliated BP, and the authors believe that this method results in stronger environmental stability compared to the use of aryl diazonium [53]. For another functionaliza-

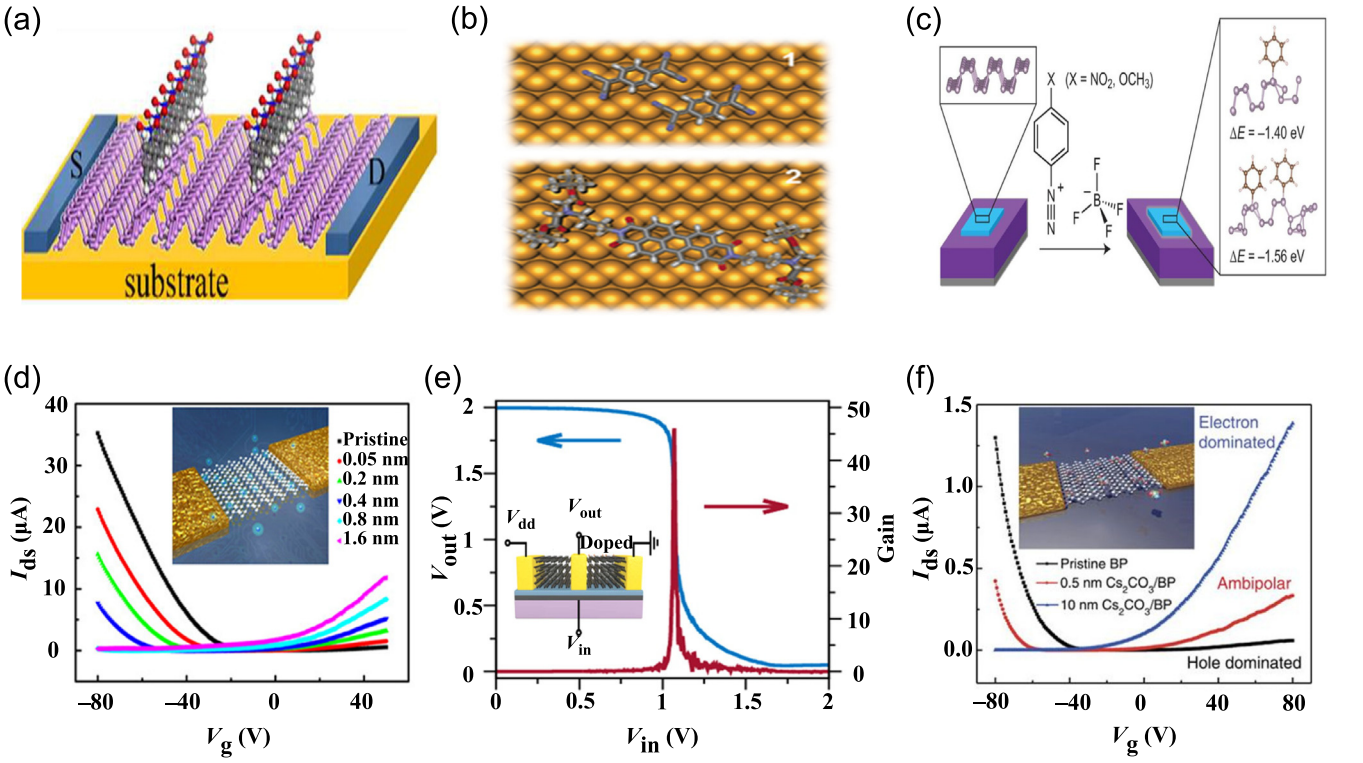

Fig. 5. The schematic diagram of functionalization and doping and its effect on BP transistors. Schematic representation of non-covalent (a) and covalent functionalization (b) of BP. Reprinted with permission from Ref. [48,49]. Copyright © 2016, John Wiley and Sons. Copyright © 2016, American Chemical Society. (c) Reaction scheme of benzenediazonium tetrafluoroborate derivatives and mechanically exfoliated few-layer BP on a Si/SiO_2 substrate. The left inset shows the pristine structure of BP and the right inset shows DFT-calculated structures of the thermodynamically favoured covalent bonding of aryl groups to BP. Reprinted with permission from Ref. [39]. Copyright © 2016, Springer Nature. (d) Linear plot of the same transfer characteristics. Inset: schematic illustration of BP devices during the deposition of K. Reprinted with permission from Ref. [50]. Copyright © 2017, American Chemical Society. (e) Output voltage, V_{out}, versus input voltage, V_{in}, of the inverter at V_{DD} = 2 V. The inverter gain versus V_{in} is shown in red on the right axis. Inset: schematic illustration of complementary inverter. Reprinted with permission from Ref. [51]. Copyright © 2016, American Chemical Society. (f) Linear plot of the transfer curves at 0.5 and 10 nm Cs_2CO_3 coverage with respect to the pristine BP. Inset: schematic illustration of BP device coated by Cs_2CO_3. Reprinted with permission from Ref. [52]. Copyright © 2015, Springer Nature.

tion method, non-covalent functionalization is usually achieved by vdW interactions. 7,7,8,8-tetracyano-*p*-quinodimethane (TCNQ), anthraquinone and benzyl viologen (BV) have been employed for non-covalent functionalization of BP in succession, and these compounds can protect BP from degradation [48,54,55]. However, there are currently no reports of specific electronic devices being fabricated to characterize the effect of non-covalent functionalization of BP.

Referring to the previous literature, doping can be also simply divided into metallic doping and non-metallic doping. Alkali metals are often employed as a dopant thanks to their relatively low electron affinities [35,50]. For example, lithium was introduced to realize low contact resistance high performance transistors [35]. In addition, high performance complementary devices have been successfully fabricated by in situ surface modification with potassium. As shown in Fig. 5d, by precisely controlling the thickness of the K layer, the hole-dominated transfer characteristics of the pristine BP can be modulated to electron-dominated behavior. In other words, BP transistors can be transformed from p-type to n-type. On the basis of the obtained results, both PN diodes and logic inverters have been demonstrated. Meanwhile, an ideality factor of 1.007 and gain of 5 could be extracted [50]. Besides, transition metals such as copper, silver, scandium etc. also can be utilized in the doping of BP [51,56,57]. Among them, Ag and Sc are often utilized to protect BP from ambient degeneration with a slight change in its electrical performance [49,53]. However, the V_{th} under n-type conditions can be modulated by Cu doping, so a complementary inverter was demonstrated by utilizing a Cu doped n-channel and a pristine p-channel, as shown in Fig. 5e. An ultra-high gain of 46 could be obtained, indicating that BP has great potential for applications in future complementary metal oxide semiconductor (CMOS) integrated circuits. There have also been some reports focused on the doping of BP by some other metals such as aluminum, germanium, tellurium [58–60]. Specifically, Al atoms can transform the pristine p-type conductivity of BP into n-type conductivity and a record high electron mobility of >1,495 $cm^2/(V\,s)$ was achieved at 260 K. Te-doped FET devices were found to maintain a high mobility of over 200 $cm^2/(V\,s)$ after three weeks' exposure to air. And after employing Ge, the contact resistance extracted by the transfer length method was 0.365 kΩ μm, which is the lowest recorded for in BP transistors without degradation of the I_{on}/I_{off} ratio. Next, non-metallic doping will be discussed in detail. Non-metallic elements and some oxides/nitrides have been introduced as dopants [54,52,55,61,62]. The transfer curves of transistors with 0.5 and 10 nm of cesium carbonate (Cs_2CO_3) compared to the pristine BP are displayed in Fig. 5f, indicating either balanced ambipolar or even n-type FET characteristics. In contrast, a hole-doping effect can be achieved with molybdenum oxide (MoO_3). Through functionalization or doping, the properties of the material can be effectively adjusted to provide reliable support for large-scale application of BP electronic devices in the future.

3.3. Superlattices

In addition to traditional methods, artificial superlattices are considered to be an effective way to go beyond the properties of the material itself [63]. Especially for the emerging 2D materials, based on the essence of the interlayer vdW interactions, artificial superlattices can be realized by layer-by-layer exfoliation and restacking [64], but the low productivity and repeatability of those methods have so far prevented their use for practical application. Thus, chemical vapor deposition (CVD) was therefore introduced to generate highly reproducible heterojunctions. However, it is increasingly difficult to obtain high-order superlattices [65]. In addition, alkali metal elements can also be employed to prepare superlattices by intercalation between two-dimensional crystals. However, this method usually leads to severe damage to the electrical properties and structural instability in most cases [66]. Recently, Wang et al. [67] introduced a stable electrochemical intercalation method of producing artificial superlattices and successfully fabricated monolayer atomic crystals alternating with molecular layers. Monolayer phosphorene molecular superlattices (MPMS) can be produced by integrating a monolayer of BP with cetyl-trimethyl ammonium bromide (CTAB). A view of the simulated atomic structure of MPMS by density functional theory (DFT) calculations is shown in Fig. 6a. High resolution cross-sectional TEM images of pristine BP and MPMS are displayed in Fig. 6b and c, respectively. The interlayer distance of pristine BP is 5.24 Å. After CTAB interpolation, the distance increased to 11.21 Å, corresponding to the DFT calculated value of 11.41 Å.

To characterize the performance of the superlattices, the same back-gated BP and MPMS FETs before and after the intercalation process were comprehensively investigated. The transfer characteristics at V_{ds} = 0.01 V are displayed in Fig. 6d, which show an enormous increase in the on/off ratio (from <10 to >10^7) after intercalation. Although the post-treatment field effect mobility dropped from 721 to 328 $cm^2/(V\,s)$, this mobility value is still comparable to that of 5–15 nm thick untreated BP and close to the theoretical limit of monolayer phosphorene (250–400 $cm^2/(V\,s)$) [68]. Then, the transport properties of the FETs were also studied from 300 to 1.9 K, as shown in Fig. 6e. The inset of Fig. 6e displays the mobility variation with temperature. The field effect mobility increased from 289 to 599 $cm^2/(V\,s)$ with decreasing temperature form 300 to 1.9 K. In the temperature zone dominated by phonon scattering, a power-law dependence with a positive exponent of 0.73 indicates that the mobility can be explained by the conventional model [69]. Furthermore, the stability of BP and MPMS FETs with a similar on-current were compared, and the results are shown in Fig. 6f. Under ambient conditions, a serious degradation can be observed in pristine BP devices after only 20–30 h, whereas, the performance of MPMS devices only showed slight degradation after 300 h. It is obvious that the stability under ambient conditions was greatly increased after the encapsulation of monolayer phosphorene between molecular monolayers due to slower oxygen and water diffusion. Experimental data show that the MPMS structure retained all the key properties of monolayer phosphorene, including high mobility, high on/off ratio, large bandgap and superior stability, which can open up new opportunities for future BP electronics.

4. Device design

The performance of BP-based electronics that has been reported is far from the theoretically predicted performance, which will greatly limit BP applications. The cause of this problem is most likely insufficient design of the device structure and incomplete processing. In order to obtain high-performance electronic devices, many strategies have been employed, including dielectric engineering, contact engineering and stability enhancement, which will be discussed detail in this section.

4.1. Contact engineering

It is well known that metal-semiconductor contact typically generates a Schottky barrier at the interface due to the location of the Fermi level. For conventional semiconductors represented by silicon, heavy doping of semiconductors by ion implantation was usually employed to solve this problem. However, for emerging two-dimensional materials, heavy doping usually degrades its properties as result of its atomic thickness. For this reason, new

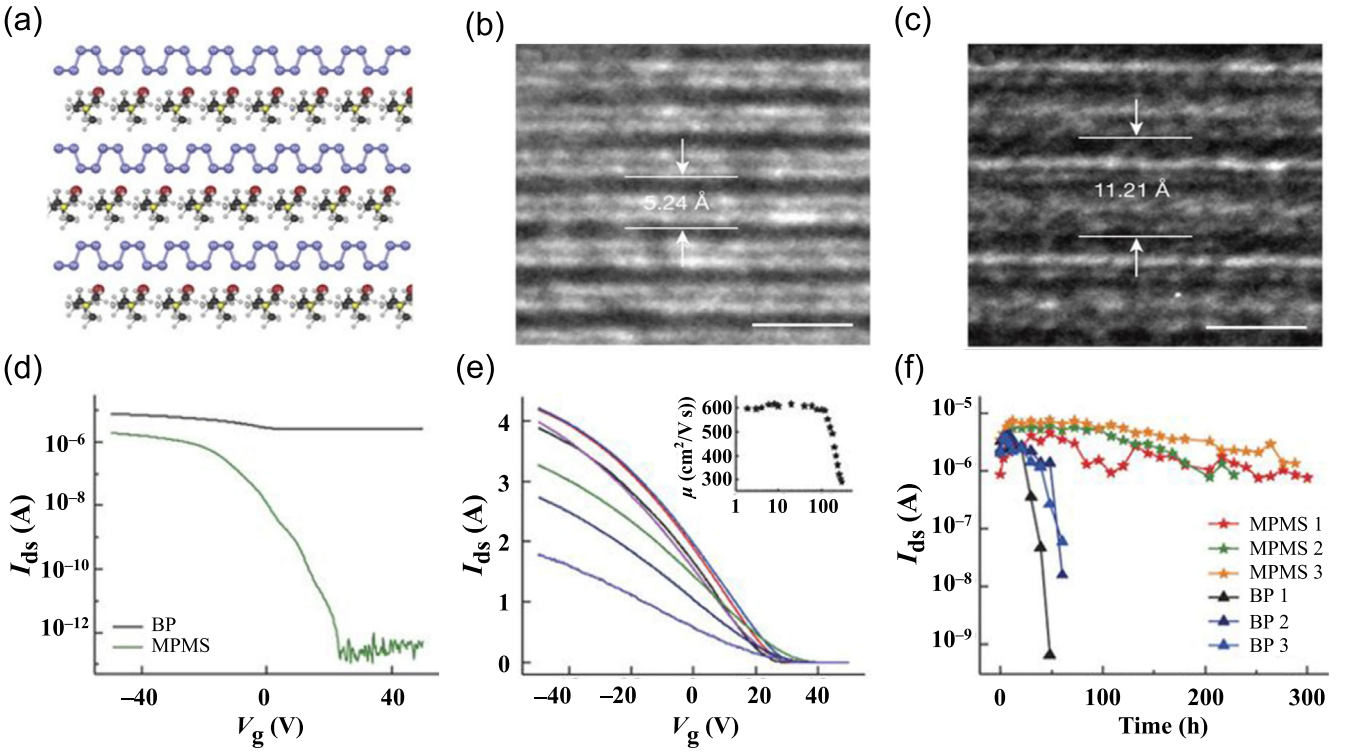

Fig. 6. The structures and performances of the BP superlattices. (a) Views of the simulated atomic structure of MPMS. The high resolution cross-sectional TEM images of BP (b) and MPMS (c). Scale bars: 1 nm. (d) Transfer characteristics at V_{ds} = 0.01 V show an on/off ratio > 10^7 in MPMS versus <10 in BP. (e) Transfer characteristics of MPMS at various temperatures from 1.9 to 300 K. Insets: mobility versus temperature. (f) Comparison of electrical stability between three MPMS (stars) and three BP (triangles) devices with similar starting on-current. Reprinted with permission from Ref. [67]. Copyright © 2018, Springer Nature.

strategies should be developed to modulate the Schottky barrier, thus optimizing metal-semiconductor contact interfaces for future electronics. To solve the problem of metal-semiconductor contact, a Schottky barrier model needs to be built to understand its impact on transport [70]. Calculated transfer characteristics of a typical Schottky barrier metal-oxide semiconductor field-effect transistor (SB-MOSFET) are shown in Fig. 7a. The calculation was performed at V_{ds} = 50 mV, and the electron and hole Schottky barrier heights (n-SBH $\varnothing^n_{sbh}$ and p-SBH $\varnothing^n_{sbh}$) were found to be 0.7 and 0.3, respectively. The total current (I_{ds}) can be divided into two parts: electron current ($I_{electron}$) and hole current (I_{hole}). Both the $I_{electron}$ and I_{hole} branches can be broken up into two separate regions, the thermal region and the tunneling region, separated by a transition point called the flat band voltage (V_{fb}). Through an in-depth understanding of the conduction process, a simple modeling approach has been proposed to quantitatively describe the transfer characteristics of SB-MOSFETs made from 2D materials, and it provides a solid theoretical foundation for follow-up studies.

Generally, the influence of different metals has been most throughly investigated. Theoretical calculations show that the five metal surfaces of Cu(1 1 1), Zn(0001), In(1 1 0), Ta(1 1 0), and Nb (1 1 0) have minimal lattice mismatch with monolayer BP [74]. Among them, Cu(1 1 1) is the best candidate to form excellent Ohmic contact with monolayer BP. Additionally, Ta(1 1 0) and Nb (1 1 0) can form strong covalent bonds with monolayer BP, and then they can form an excellent interface to the second layer. Notably, the authors found that the freestanding BP channel is n-type, which is different from the conventional characteristics of BP FETs. Different work function metals have been used in order to form optimized interfaces. Fig. 7b demonstrates the n-SBH and p-SBH of several metals with an atomic layer deposition (ALD) Al_2O_3 capping layer [75]. The results show Fermi level pinning for Ti, Ni, and Ag. On the other hand, for the low work function metals (Sc and Er), the intermixing of a layer with the metal oxide may lead to Fermi level depinning and hence separate the values of the n-SBH and p-SBH. Remarkably, a record high current density of 580 μA/μm was achieved using a Sc contact [76]. Apart from this, ferromagnetic metals have also been employed to optimize contact, such as cobalt, permalloy, and a low contact resistance of ~0.31 kΩ μm was realized by Py contacts [77,78]. Palladium (Pd) was reported to have high hydrogen solubility. Thus, it has been employed to reduce the SBH of BP FETs [71]. The contact resistance of Pd-contacted few-layer BP FET with different H_2 concentrations is displayed in Fig. 7c. The contact resistance (R_c) improved from ~7.10 to ~1.05 kΩ μm under a suitable H_2 concentration. Contemporaneously, vdW contacts have also been introduced to improve contact quality [72,79–81]. After applying an h-BN film to the Co/BP interface, strong n-type conduction was observed as a consequence of reducing the work function of the Co/h-BN contact [82]. Fig. 7d exhibits four- and two-terminal field effect mobility of a Co/h-BN contacted BP device as a function of temperature. The mobility of the Co/h-BN contact increased monotonically from ~245 to ~4,190 cm^2/(V s) with decreasing temperature from 300 to 40 K measured by four-terminal geometry (4 T). Two-terminal geometry (2 T) measurements were also performed, as shown at the bottom of Fig. 7d. For comparison purposes, the performance of a graphene contacted device (similar thickness) is also plotted in the figure [83]. It should be noted that the mobility measured with 2 T is an order of magnitude smaller than that measured with 4 T due to the presence of contact resistance. In addition to the candidates for replacement contacts, post-treatment with vacuum annealing can also achieve reduced contact resistance [73,76,84]. As plotted in Fig. 7e, the contact resistance will be greatly reduced by optimizing the annealing temperature and can reach an ultra-

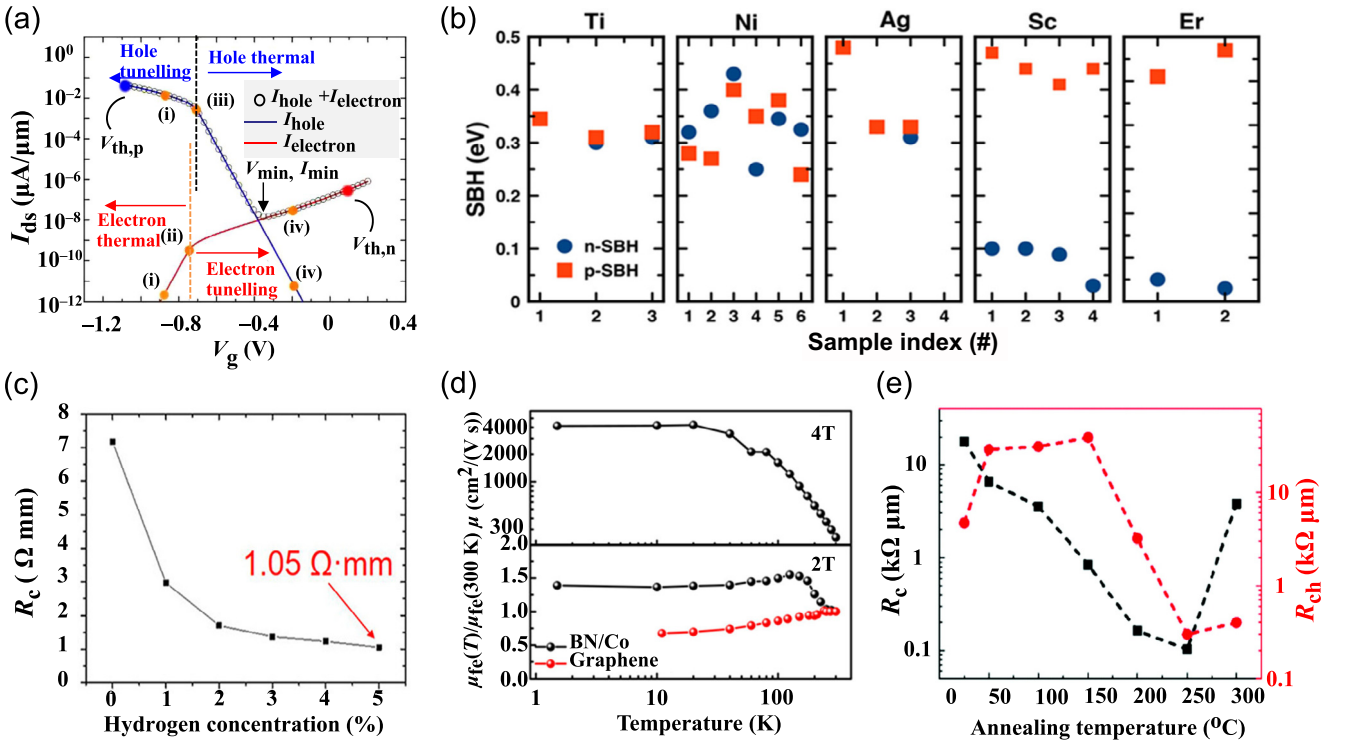

Fig. 7. The influence of contact interface on the performance of BP transistors. (a) The calculated transfer characteristic of an SB-MOSFET for V_{ds} = −50 mV with $\varnothing^{p}_{sbh}$ = 0.3 eV and $\varnothing^{n}_{sbh}$ = 0.7 eV. The total current, I_{ds} (open circles) is the sum of $I_{electron}$ and I_{hole}, plotted in red and blue, respectively. Key gate voltage (V_{gs}) points on the transfer curve are labelled (i)–(iv). Reprinted with permission from Ref. [70]. Copyright © 2015, Springer Nature. (b) A summary of the extracted Schottky barrier height (n-SBH, p-SBH) on Ni, Ag, Ti, Sc, and Er with ALD Al_2O_3 capping. Reprinted with permission from Ref. [68]. Copyright © 2016, American Physical Society. (c) Contact resistance of Pd-contacted few-layer BP FET under different H_2 concentrations. Reprinted with permission from Ref. [71]. Copyright © 2017, American Chemical Society. (d) Four- and two-terminal field effect mobility of Co/h-BN contacted BP device as a function of temperature. For comparison purposes, performance of graphene contacted BP (similar thickness) is also plotted. Reprinted with permission from Ref. [72]. Copyright © 2018, Springer Nature. (e) The contact resistance (R_c) and channel resistance (R_{ch}) of the BP FETs at different low-vacuum annealing temperatures. Reprinted with permission from Ref. [73]. Copyright © 2018, Royal Society of Chemistry.

low value of 0.103 kΩ μm. Hence, a large number of strategies have been developed to improve the contacts of BP FETs, and they have had a great effect on performance, but for industrialization, there is still much to be done.

4.2. Dielectric engineering

Dielectric engineering is important for transistors because the performance of SiO_2-supported devices is severely affected by interface scattering, including oxide trapped charges, surface roughness, and surface optical phonons [31,85–89]. A SiO_2 substrate can be completely replaced by other dielectrics for the purpose of minimizing this degradation. The use of high-k dielectrics is the simplest and most effective way to achieve this goal. As shown in the inset of Fig. 8a, a novel dielectric HfLaO has been exploited to replace native SiO_2 [90]. The transfer characteristics of devices with the same channel length using SiO_2 and HfLaO dielectrics with V_{ds} = −0.05 V are plotted in Fig. 8a. It can be clearly observed that the SS has been enormously improved after replacing the dielectric. Replacement of SiO_2 with HfO_2 has also been investigated in the same structure [34], and the maximum drain current density was found to reach 480 and 906 μA/μm at 300 and 20 K, respectively. The transfer characteristics of BP on both SiO_2 and HfO_2 at different temperatures with V_{ds} = −0.05 V are displayed in Fig. 8b and c, and much tighter electrostatic control can be observed in HfO_2 dielectric devices. Notably, the gate voltage corresponding to the minimum current for SiO_2-supported devices shifted greatly from 35 to 20 V as the temperature was decreased to 70 K, while it changed only slightly for HfO_2-supported devices, indicating frozen trap charges at the oxide/BP interface at low temperature. Furthermore, high-k dielectrics have also been employed to passivate the upper surface of BP to reduce scattering [36,91,93,94]. Near ideal SS values were successfully achieved at room temperature by improving the BP/HfO_2 interface quality with thermal treatments [94,95]. Particularly, a record drain current exceeding 1 A/mm has been achieved by integrating 3 nm of HfO_2 and 20 nm of ZrO_2 [93]. Apart from HfO_2, Al_2O_3 has also been proven to reduce current fluctuations [91], as shown in Fig. 8d. Moreover, passivation of BP with native phosphorus oxide (PO_x) grown by oxygen plasma is known to improve the performance of exfoliated BP flakes, and Al_2O_3 was integrated with PO_x to realize a room temperature top-gate mobility of 115 cm^2/(V s) due to the low defect density of the BP/PO_x interface [96].

However, charge traps and surface optical phonon scattering arise from the application of high-k dielectrics. Thus, h-BN is considered as a good candidate to achieve a good interface owing to its advantages of atomic smoothness and large surface optical phonon energy, which most probably minimize the unfavorable effects of optical phonon scattering and trapped charges. By applying an h-BN/Al_2O_3 bilayer gate dielectric, a gate leakage of less than 10^{-12} A/μm^2 (V_{gs} = −1 V) could be obtained with an effective oxide thickness of 3 nm [36]. Chen et al. [69] demonstrated a sandwich structure with BP encapsulated between h-BN layers, which achieved hysteresis-free and a high mobility of 1,350 cm^2/(V s), as plotted in Fig. 8e. In their group's follow-up work, a record room temperature mobility of 5,200 cm^2/(V s) was realized with the same structure fabricated in vacuum [92]. Fig. 8f shows the cryogenic temperature (2 K) conductance-gate voltage characteristics (V_{ds} = 1 mV, line) and FET mobility at varying gate voltages (dots). At low temperature, a mobility of 45,000 cm^2/(V s) can be

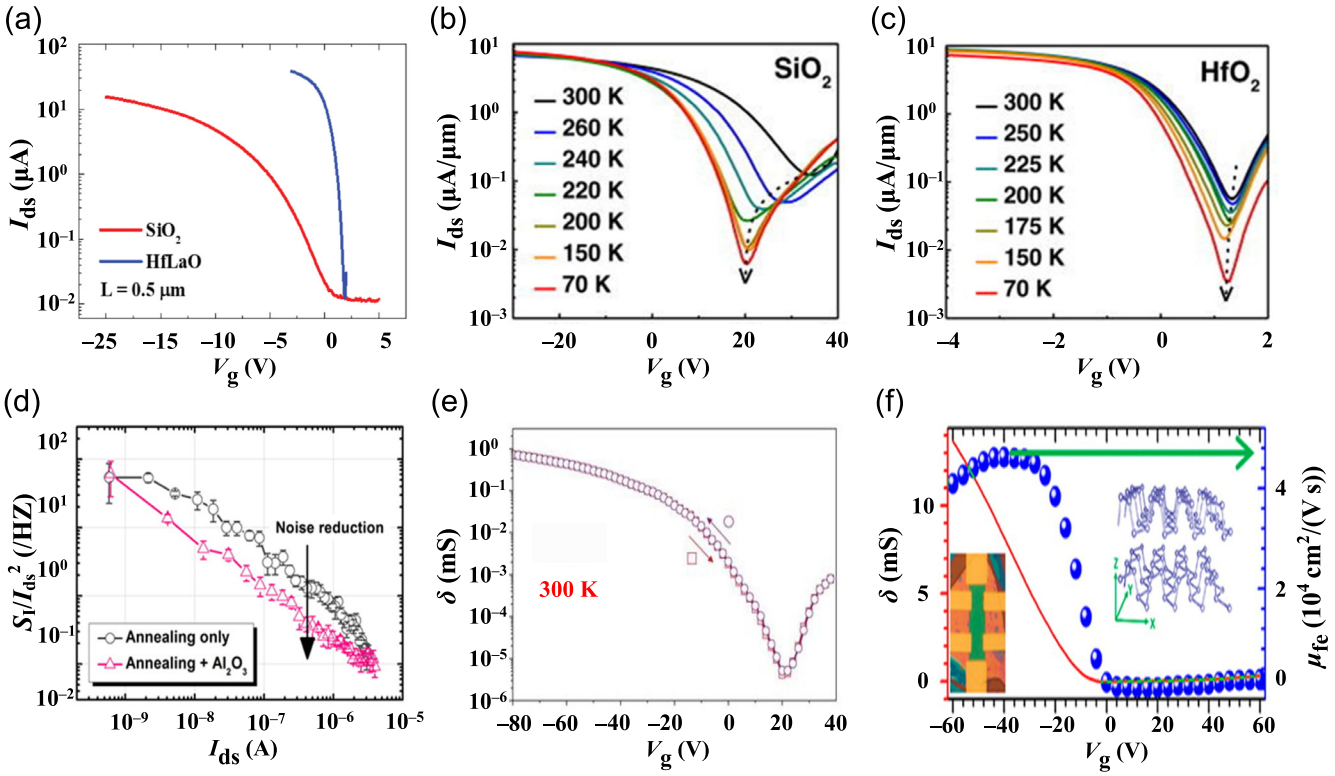

Fig. 8. (Color online) The influence of dielectric engineering on the performance of BP transistors. (a) Transfer characteristics of the same channel length device with SiO_2 and HfLaO dielectrics at 300 K with $V_{ds} = -0.05$ V. Inset: schematic of device structure. Reprinted with permission from Ref. [90]. Copyright © 2018, IEEE. (b and c) Transfer characteristics of 500 nm device for BP on SiO_2 and HfO_2 at different temperatures with $V_{ds} = -0.05$ V. Reprinted with permission from Ref. [34]. Copyright © 2017, AIP Publishing. (d) Noise reduction due to Al_2O_3 passivation represented by the mean normalized drain spectral density as a function of the drain current before and after the Al_2O_3 passivation. Reprinted with permission from Ref. [91]. Copyright © 2014, American Chemical Society. (e) The room temperature conductivity showing hysteresis free of the h-BN–BP–h-BN hetero-structure devices. Reprinted with permission from Ref. [69]. Copyright © 2015, Springer Nature. (f) Cryogenic temperature (2 K) conductance-gate voltage characteristics ($V_{ds} = 1$ mV, line) and field effect mobility at varying gate voltages (dots). Inset: the left panel shows an optical micrograph of a typical BP FETs, The right panel shows the atomic structure of BP. Reprinted with permission from Ref. [92]. Copyright © 2016, American Chemical Society.

observed, and this is the maximum value observed so far. Moreover, in high electric field operation, h-BN has been proven to effectively cool devices when self-heating is obvious [97]. The superior performance of high-k dielectrics and h-BN in dielectric engineering has been proven by many researchers. It is believed that the integration of h-BN and high-k dielectrics to achieve high-quality interfaces will provide reliable support for future applications of BP electronic devices.

4.3. Stability

The application of BP electronics is mainly limited by instability caused by their extraordinarily high surface areas, which enhances chemical reactivity with the external environment [98]. In order to clarify the root causes of BP device degradation, a comprehensive study combining theory and experiment has been reported [99]. Fig. 9a and b show 2D electron energy loss spectra taken using a scanning tunneling electron microscope (STEM-EELS) of a BP flake immediately after exfoliation and exposure to air for 1 d, respectively. The reduction of BP thickness can be clearly seen from the figure, indicating that the morphology is changed after exposing BP to air. However, no changes in the morphology of the were observed BP sample after exposure to H_2O. Then, contact angle measurements were performed, which revealed that the pristine hydrophobic BP surface was turned progressively hydrophilic by oxidation, as shown in Fig. 9c and d. Experimental and theoretical analysis showed that the degradation of BP is mainly caused by the interaction with oxygen, while water does not play a primary role.

After fully understanding the root causes of BP degradation, many strategies have been attempted to achieve more stable BP devices. These strategies can be roughly divided into three types, as summarized in Table 1, including functionalization, doping, and passivation. (1) In functionalization approach, Ag, benzyl viologen (BV), and H_2 can be employed as functionalization dopants to enhance the stability of BP devices. Ag^+ can be spontaneously adsorbed on the BP surface, and hence render BP more stable in ambient condition [56]. AFM images of BP before and after absorbing Ag^+ are shown in Fig. 9e, and it can be clearly seen that the treated BP showed stronger stability. After BV treatment, BP transistors not only can balance their p-n type, but also can maintain good hole mobility and electron mobility after 250 h [55]. The surface morphology of BP treated by H_2 can be maintained for 4 weeks with only a 15% decrease in mobility and on/off ratio [101]. (2) As for doping, Te, Li, and S are commonly utilized and form covalent bonds with BP thereby enhancing its stability. A Te-doped sample can effectively inhibit the formation of phosphoric acids, which was proved by ^{31}P magic angle spinning (MAS) nuclear magnetic resonance (NMR) measurements [59]. By chemically intercalating BP with LiH, the deactivation of oxygen-reactive defects in the near surface regions can be suppressed so that the degradation of BP is hindered [100]. S atoms energetically prefer to chemisorb on the BP surface in a dangling form, and this leads a lower degradation rate of S-doped BP [61]. (3) Passivation can be introduced in two ways: immediate passivation and passivation after removing bubbles. Immediate passivation is usually carried out using oxides or a combination of oxides with other materials. AlO_x deposited by ALD has been applied to effectively suppress ambient degradation

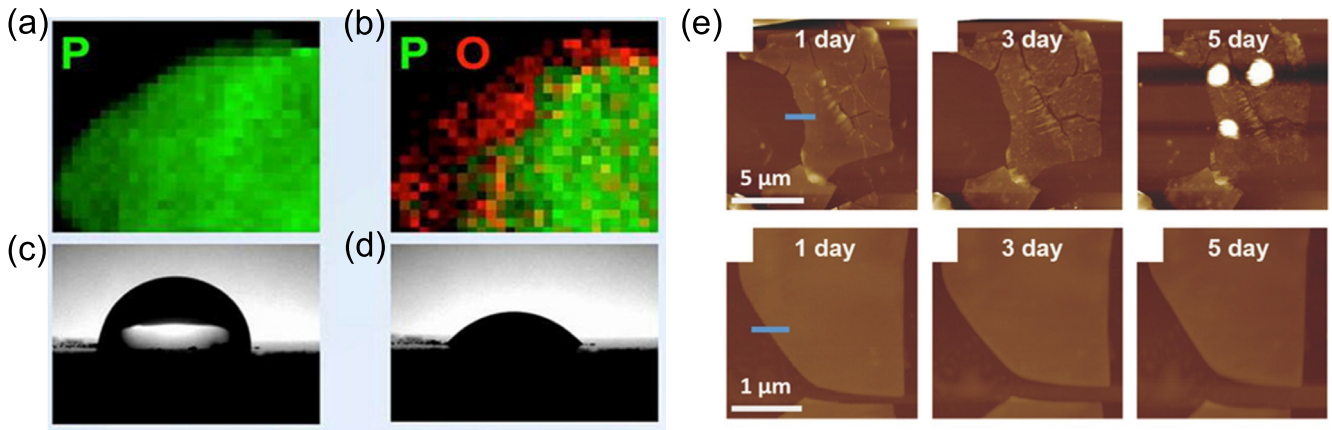

Fig. 9. The cause of BP instability and the effect of improvement. 2D STEM-EELS map of the BP flake immediately after exfoliation (a) and after exposure (b) to air for 1 d, respectively. P is shown in green; O in red. (c and d) Time-dependent sessile drop contact angle measurement for oxygen-containing water in contact with freshly exfoliated BP. Scale bar: 2 mm. Reprinted with permission from Ref. [99]. Copyright © 2016, American Chemical Society. (e) AFM images of a bare BP sheet exposed to air for 1, 3, and 5 d and AFM images (top) and a BP-Ag^+ sheet exposed to air for 1, 3, and 5 d (bottom). Reprinted with permission from Ref. [56]. Copyright © 2017, John Wiley and Sons.

Table 1
Summarize the means to effectively enhance BP stability.

Means	Method	Properties	Refs.
Functionalization	Ag^+	Transport properties are maintained in the first 60 h and only a slight decline is observed in the next 12 h	[55]
	Benzyl viologen (BV)	Hole mobility can sustain steadily with electron mobility shows a slight decrease after 250 h	[49]
	H	The average values of mobility and I_{on}/I_{off} ratio still keep ≈85% after 28 d	[97]
Doping	Te	Maintain high mobility of over 200 $cm^2/(V\ s)$ (30% of the initial value) after three weeks, undoped ones ~ 2% of the initial value	[56]
	Li and hydrogenation	The 9% decrease in mobility over a period of 18 d	[98]
	Sulfur (S)	After exposing to air for 21 d, the charge-carrier mobility remained as high as 77.4% and a large I_{on}/I_{off} ratio of ~10^3 is still retained	[58]
Passivation	Hydrophobic fluoropolymer Al_2O_3	Best preservation of I_{on}/I_{off} ratio, with negligible change after 79 d	[100]
	AlO_x	Maintain high on/off ratios of ~10^3 and mobility of ~100 $cm^2/(V\ s)$ for over 2 weeks in ambient conditions	[99]
	(~5 nm) BN And Al_2O_3	Protected from degradation in ambient for over 6 months	[101]
	Native surface Phosphorus oxide	Hole (electron) mobility of 233 (94) $cm^2/(V\ s)$ slightly decreased to 200 (82) $cm^2/(V\ s)$ after 30 d under ambient condition.	[102]
	1,2-Ethanedithiol (EDT) hBN	Retained without changing device characteristics even when exposed to 30 d in air. Especially, EDT can recover device characteristics	[103]
	Ar plsma PMMA	~80% degrade of I_{on} after one week	[104]

[102]. Immediately after deposition, a hydrophobic fluoropolymer and h-BN are introduced to combine with Al_2O_3 [103,104]. Notably, Gamage et al. [104] claim that 1.6 nm of h-BN and 4 nm of Al_2O_3 can protect BP from degradation in ambient conditions for over 6 months. Passivation after removing bubbles means to use some processes to move any of the BP that has been oxidized on the surface. Processes that have been reported include thermal etching methods [105], plasma etching [106], and 1,2-ethanedithiol (EDT) treatment [107]. Among them, thermal etching methods can control the BP thickness and form a native surface phosphorus oxide, which can preserve the performance of BP devices for 1 month. In addition, the exposed oxidized BP surface can be removed by plasma etching, followed immediately by polymethyl methacrylate (PMMA) passivation. Environmental stability over several weeks was obtained. It is worth noting that the 1,2-ethanedithiol (EDT) treatment was not only a simple and effective way to remove the bubbles but it also can recover the performance of degraded BP devices. The EDT-induced recovering effect will allow a new path for the optimization of BP electronics. Although so many strategies have been introduced to enhance the stability of BP, so far, there is still no effective way to maintain the performance of BP devices for a long time. More effort needs to be invested to solve this problem that plagues all scientists working in this field.

5. Summary and perspective

In this review, the basic structural and electronic characteristics of BP, performance modulation strategies and electronics design were discussed in detail. BP has great potential for application in next-generation electronic devices due to its superior performance. To achieve this goal, researchers have done rigorous work on high-performance, high-stability electronic devices using BP, investigating all aspects from its basic properties to device structure optimization. Through these efforts, researchers have gradually increased our understanding of BP and improved the corresponding device performance in many ways. However, to promote the industrialization of BP electronics, the existing results are far from sufficient. We need to conduct more in-depth research in the following areas: (1) Synthesize high-quality wafer-scale crystalline. Until now, wafer-scale BP films have not been successfully prepared, but wafer-scale films are indispensable for large-scale applications. Therefore, the preparation of wafer-scale high-quality BP films requires further research. (2) Optimize interface quality. Although extensive research has been conducted on contact and dielectric engineering, the interface still needs further optimization, and simple and reliable strategies need to be developed to achieve lower contact resistance and higher interface quality. (3) Enhance device

stability. Stability is one of our most important concerns. Several reports focusing on BP stability have been published, but there is still no way to maintain the performance of BP electronics sufficiently long for practical applications. These serious problems greatly limit further development of BP electronics, and more new strategies are needed to make BP sufficiently robust to withstand the deterioration caused by the external environment.

Conflict of interest

The authors declare that they have no conflict of interest.

Acknowledgment

This work was supported by the National Key Research and Development Program of Ministry of Science and Technology of China (2018YFB0406603), the National Natural Science Foundation of China (61811540408, 51872084, 61704051, 61574101, and U1632156), the Strategic Priority Research Program of Chinese Academy of Sciences (XDB30000000), and the Natural Science Foundation of Hunan Province (2017RS3021, 2017JJ3033).

Author contributions

Hao Huang wrote the whole manuscript. Bei Jiang assisted in collecting relevant literatures. Xuming Zou helped to amend the full manuscript. Xingzhong Zhao checked the manuscript. Lei Liao confirmed the structure of the manuscript and revised the full text.

References

[1] Waldrop MM. The semiconductor industry will soon abandon its pursuit of Moore's law. Now things could get a lot more interesting. Nature 2016;530:144–7.
[2] Duan XD, Wang C, Pan AL, et al. Two-dimensional transition metal dichalcogenides as atomically thin semiconductors: opportunities and challenges. Chem Soc Rev 2015;44:8859–76.
[3] Kawaura H, Sakamoto T, Baba T. Observation of source-to-drain direct tunneling current in 8 nm gate electrically variable shallow junction metal-oxide-semiconductor field-effect transistors. Appl Phys Lett 2000;76:3810–2.
[4] Novoselov KS, Geim AK, Morozov SV, et al. Electric field effect in atomically thin carbon films. Science 2004;306:666–9.
[5] Novoselov KS, Jiang D, Schedin F, et al. Two-dimensional atomic crystals. Proc Natl Acad Sci USA 2005;102:10451–3.
[6] Geim AK, Grigorieva IV. Van der waals heterostructures. Nature 2013;499:419–25.
[7] Radisavljevic B, Radenovic A, Brivio J, et al. Single-layer MoS_2 transistors. Nat Nanotechnol 2011;6:147–50.
[8] Li L, Yu Y, Ye GJ, et al. Black phosphorus field-effect transistors. Nat Nanotechnol 2014;9:372–7.
[9] Bridgman PW. Two new modifications of phosphorus. J Franklin I 1914;178:644.
[10] Li X, Xiong X, Wu Y. Toward high-performance two-dimensional black phosphorus electronic and optoelectronic devices. Chin Phys B 2017;26:037307.
[11] Zhou Y, Zhang M, Guo Z, et al. Recent advances in black phosphorus-based photonics, electronics, sensors and energy devices. Mater Horiz 2017;4:997–1019.
[12] Lei W, Liu G, Zhang J, et al. Black phosphorus nanostructures: recent advances in hybridization, doping and functionalization. Chem Soc Rev 2017;46:3492–509.
[13] Du H, Lin X, Xu Z, et al. Recent developments in black phosphorus transistors. J Mater Chem C 2015;3:8760–75.
[14] Liu H, Du Y, Deng Y, et al. Semiconducting black phosphorus: synthesis, transport properties and electronic applications. Chem Soc Rev 2015;44:2732–43.
[15] Ling X, Wang H, Huang S, et al. The renaissance of black phosphorus. Proc Natl Acad Sci USA 2015;112:4523–30.
[16] Tran V, Soklaski R, Liang Y, et al. Layer-controlled band gap and anisotropic excitons in few-layer black phosphorus. Phys Rev B 2014;89:235319.
[17] Das S, Zhang W, Demarteau M, et al. Tunable transport gap in phosphorene. Nano Lett 2014;14:5733–9.
[18] Jiang B, Zou X, Su J, et al. Impact of thickness on contact issues for pinning effect in black phosphorus field-effect transistors. Adv Funct Mater 2018;28:1801398.
[19] Li XS, Cai WW, An JH, et al. Large-area synthesis of high-quality and uniform graphene films on copper foils. Science 2009;324:1312–4.
[20] Dean CR, Young AF, Meric I, et al. Boron nitride substrates for high-quality graphene electronics. Nat Nanotechnol 2010;5:722–6.
[21] Berger C, Song ZM, Li TB, et al. Ultrathin epitaxial graphite: 2D electron gas properties and a route toward graphene-based nanoelectronics. J Phys Chem B 2004;108:19912–6.
[22] Liu Y, Cheng R, Liao L, et al. Plasmon resonance enhanced multicolour photodetection by graphene. Nat Commun 2011;2:579.
[23] Bolotin KI, Sikes KJ, Jiang Z, et al. Ultrahigh electron mobility in suspended graphene. Solid State Commun 2008;146:351–5.
[24] Liao L, Bai J, Qu Y, et al. High-kappa oxide nanoribbons as gate dielectrics for high mobility top-gated graphene transistors. Proc Natl Acad Sci USA 2010;107:6711–5.
[25] Wang X, Wang P, Wang J, et al. Ultrasensitive and broadband MoS_2 photodetector driven by ferroelectrics. Adv Mater 2015;27:6575–81.
[26] Yang L, Majumdar K, Liu H, et al. Chloride molecular doping technique on 2D materials: WS_2 and MoS_2. Nano Lett 2014;14:6275–80.
[27] Wang J, Yao Q, Huang CW, et al. High mobility MoS_2 transistor with low Schottky barrier contact by using atomic thick h-BN as a tunneling layer. Adv Mater 2016;28:8302–8.
[28] Wang J, Li S, Zou X, et al. Integration of high-k oxide on MoS_2 by using ozone pretreatment for high-performance MoS_2 top-gated transistor with thickness-dependent carrier scattering investigation. Small 2015;11:5932–8.
[29] Yang Z, Liu X, Zou X, et al. Performance limits of the self-aligned nanowire top-gated MoS_2 transistors. Adv Funct Mater 2017;27:1602250.
[30] Zou X, Wang J, Chiu CH, et al. Interface engineering for high-performance top-gated MoS_2 field-effect transistors. Adv Mater 2014;26:6255–61.
[31] Zou X, Huang CW, Wang L, et al. Dielectric engineering of a boron nitride/hafnium oxide heterostructure for high-performance 2D field effect transistors. Adv Mater 2016;28:2062–9.
[32] Fang H, Chuang S, Chang TC, et al. High-performance single layered WSe_2 p-FETs with chemically doped contacts. Nano Lett 2012;12:3788–92.
[33] Liu H, Neal AT, Zhu Z, et al. Phosphorene: an unexplored 2D semiconductor with a high hole mobility. ACS Nano 2014;8:4033–41.
[34] Li T, Zhang Z, Li X, et al. High field transport of high performance black phosphorus transistors. Appl Phys Lett 2017;110:163507.
[35] Gao TT, Li XF, Xiong X, et al. Optimized transport properties in lithium doped black phosphorus transistors. IEEE Electr Dev Lett 2018;39:769–72.
[36] Yang LM, Qiu G, Si MW, et al. Few-layer black phosporous pmosfets with BN/Al_2O_3 bilayer gate dielectric: achieving I_{on}=850 mA/mm, G_m = 340 mS/mm and R_c = 0.58 kΩ μm. 2016. IEEE IEDM 2016. UNSP 5.5.
[37] Luo W, Zemlyanov DY, Milligan CA, et al. Surface chemistry of black phosphorus under a controlled oxidative environment. Nanotechnology 2016;27:434002.
[38] Chang HM, Fan KL, Charnas A, et al. Experimental analysis of the schottky barrier height of metal contacts in black phosphorus field-effect transistors. J Phys D Appl Phys 2018;51:135306.
[39] Ryder CR, Wood JD, Wells SA, et al. Covalent functionalization and passivation of exfoliated black phosphorus via aryl diazonium chemistry. Nat Chem 2016;8:597–602.
[40] Wang H, Wang X, Xia F, et al. Black phosphorus radio-frequency transistors. Nano Lett 2014;14:6424–9.
[41] Zhu W, Park S, Yogeesh MN, et al. Black phosphorus flexible thin film transistors at gighertz frequencies. Nano Lett 2016;16:2301–6.
[42] Yin D, AlMutairi A, Yoon Y. Assessment of high-frequency performance limit of black phosphorus field-effect transistors. IEEE T Electron Dev 2017;64:2984–91.
[43] Singh S, Thakar K, Kaushik N, et al. Performance projections for two-dimensional materials in radio-frequency applications. Phys Rev Appl 2018;10:014022.
[44] Xia F, Wang H, Jia Y. Rediscovering black phosphorus as an anisotropic layered material for optoelectronics and electronics. Nat Commun 2014;5:4458.
[45] Liu Y, Guo J, He Q, et al. Vertical charge transport and negative transconductance in multilayer molybdenum disulfides. Nano Lett 2017;17:5495–501.
[46] Morita A. Semiconducting black phosphorus. Appl Phys A Mater 1986;39:227–42.
[47] Perebeinos V, Rotkin SV, Petrov AG, et al. The effects of substrate phonon mode scattering on transport in carbon nanotubes. Nano Lett 2009;9:312–6.
[48] Abellan G, Lloret V, Mundloch U, et al. Noncovalent functionalization of black phosphorus. Angew Chem Int Ed 2016;55:14557–62.
[49] Li Q, Zhou QH, Niu XH, et al. Covalent functionalization of black phosphorus from first-principles. J Phys Chem Lett 2016;7:4540–6.
[50] Han C, Hu Z, Gomes LC, et al. Surface functionalization of black phosphorus via potassium toward high-performance complementary devices. Nano Lett 2017;17:4122–9.
[51] Koenig SP, Doganov RA, Seixas L, et al. Electron doping of ultrathin black phosphorus with Cu adatoms. Nano Lett 2016;16:2145–51.
[52] Xiang D, Han C, Wu J, et al. Surface transfer doping induced effective modulation on ambipolar characteristics of few-layer black phosphorus. Nat Commun 2015;6:6485.
[53] van Druenen M, Davitt F, Collins T, et al. Covalent functionalization of few-layer black phosphorus using lodonium salts and comparison to diazonium modified black phosphorus. Chem Mater 2018;30:4667–74.

[54] Du YC, Yang LM, Zhou H, et al. Performance enhancement of black phosphorus field-effect transistors by chemical doping. IEEE Electr Device Lett 2016;37:429–32.
[55] Yue D, Lee D, Jang YD, et al. Passivated ambipolar black phosphorus transistors. Nanoscale 2016;8:12773–9.
[56] Guo Z, Chen S, Wang Z, et al. Metal-ion-modified black phosphorus with enhanced stability and transistor performance. Adv Mater 2017;29:1703811.
[57] Wang X, Tang C, Zhu W, et al. A new effective approach to prevent the degradation of black phosphorus: the scandium transition metal doping. J Phys Chem C 2018;122:9654–62.
[58] Prakash A, Cai Y, Zhang G, et al. Black phosphorus n-type field-effect transistor with ultrahigh electron mobility via aluminum adatoms doping. Small 2017;13:1602909.
[59] Yang B, Wan B, Zhou Q, et al. Te-doped black phosphorus field-effect transistors. Adv Mater 2016;28:9408–15.
[60] Chang HM, Charnas A, Lin YM, et al. Germanium-doped metallic ohmic contacts in black phosphorus field-effect transistors with ultra-low contact resistance. Sci Rep 2017;7:16857.
[61] Lv W, Yang B, Wang B, et al. Sulfur-doped black phosphorus field-effect transistors with enhanced stability. ACS Appl Mater Interface 2018;10:9663–8.
[62] Xu Y, Yuan J, Zhang K, et al. Field-induced n-doping of black phosphorus for cmos compatible 2D logic electronics with high electron mobility. Adv Funct Mater 2017;27:1702211.
[63] Liu Y, Weiss NO, Duan X, et al. Van der waals heterostructures and devices. Nat Rev Mater 2016. 1: UNSP 16042.
[64] Haigh SJ, Gholinia A, Jalil R, et al. Cross-sectional imaging of individual layers and buried interfaces of graphene-based heterostructures and superlattices. Nat Mater 2012;11:764–7.
[65] Duan X, Wang C, Shaw JC, et al. Lateral epitaxial growth of two-dimensional layered semiconductor heterojunctions. Nat Nanotechnol 2014;9:1024–30.
[66] Yu Y, Yang F, Lu XF, et al. Gate-tunable phase transitions in thin flakes of 1T-TaS_2. Nat Nanotechnol 2015;10:270–6.
[67] Wang C, He Q, Halim U, et al. Monolayer atomic crystal molecular superlattices. Nature 2018;555:231–6.
[68] Rudenko AN, Brener S, Katsnelson MI. Intrinsic charge carrier mobility in single-layer black phosphorus. Phys Rev Lett 2016;116:246401.
[69] Chen X, Wu Y, Wu Z, et al. High-quality sandwiched black phosphorus heterostructure and its quantum oscillations. Nat Commun 2015;6:7315.
[70] Penumatcha AV, Salazar RB, Appenzeller J. Analysing black phosphorus transistors using an analytic Schottky barrier MOSFET model. Nat Commun 2015;6:8948.
[71] Ma Y, Shen C, Zhang A, et al. Black phosphorus field-effect transistors with work function tunable contacts. ACS Nano 2017;11:7126–33.
[72] Liu Y, Guo J, Zhu E, et al. Approaching the schottky-mott limit in van der waals metal-semiconductor junctions. Nature 2018;557:696–700.
[73] Park H, Son J, Kim J. Reducing the contact and channel resistances of black phosphorus via low-temperature vacuum annealing. J Mater Chem C 2018;6:1567–72.
[74] Gong K, Zhang L, Ji W, et al. Electrical contacts to monolayer black phosphorus: a first-principles investigation. Phys Rev B 2014;90:125441.
[75] Wang CH, Incorvia JAC, McClellan CJ, et al. Unipolar n-type black phosphorus transistors with low work function contacts. Nano Lett 2018;18:2822–7.
[76] Li L, Engel M, Farmer DB, et al. High-performance p-type black phosphorus transistor with scandium contact. ACS Nano 2016;10:4672–7.
[77] Anugrah Y, Robbins MC, Crowell PA, et al. Determination of the Schottky barrier height of ferromagnetic contacts to few-layer phosphorene. Appl Phys Lett 2015;106:103108.
[78] Haratipour N, Namgung S, Grassi R, et al. High-performance black phosphorus MOSFETs using crystal orientation control and contact engineering. IEEE Electr Device Lett 2017;38:685–8.
[79] Liu Y, Guo J, Wu Y, et al. Pushing the performance limit of sub-100 nm molybdenum disulfide transistors. Nano Lett 2016;16:6337–42.
[80] Liu Y, Wu H, Cheng HC, et al. Toward barrier free contact to molybdenum disulfide using graphene electrodes. Nano Lett 2015;15:3030–4.
[81] Liu Y, Duan X, Huang Y, et al. Two-dimensional transistors beyond graphene and TMDCs. Chem Soc Rev 2018;47:6388–409.
[82] Avsar A, Tan JY, Luo X, et al. Van der waals bonded Co/h-BN contacts to ultrathin black phosphorus devices. Nano Lett 2017;17:5361–7.
[83] Avsar A, Vera-Marun IJ, Tan JY, et al. Air-stable transport in graphene-contacted, fully encapsulated ultrathin black phosphorus-based field-effect transistors. ACS Nano 2015;9:4138–45.
[84] Ling ZP, Sakar S, Mathew S, et al. Black phosphorus transistors with near band edge contact Schottky barrier. Sci Rep 2015;5:18000.
[85] Katsnelson MI, Geim AK. Electron scattering on microscopic corrugations in graphene. Philos Trans A Math Phys Eng Sci 2008;366:195–204.
[86] Chen JH, Jang C, Xiao S, et al. Intrinsic and extrinsic performance limits of graphene devices on SiO_2. Nat Nanotechnol 2008;3:206–9.
[87] Fratini S, Guinea F. Substrate-limited electron dynamics in graphene. Phys Rev B 2008;77.
[88] Hwang EH, Adam S, Sarma SD. Carrier transport in two-dimensional graphene layers. Phys Rev Lett 2007;98:186806.
[89] Morozov SV, Novoselov KS, Katsnelson MI, et al. Giant intrinsic carrier mobilities in graphene and its bilayer. Phys Rev Lett 2008;100:016602.
[90] Xiong X, Li XF, Huang MQ, et al. High performance black phosphorus electronic and photonic devices with HfLaO dielectric. IEEE Electr Device Lett 2018;39:127–30.
[91] Na J, Lee YT, Lim JA, et al. Few-layer black phosphorus field-effect transistors with reduced current fluctuation. ACS Nano 2014;8:11753–62.
[92] Long G, Maryenko D, Shen J, et al. Achieving ultrahigh carrier mobility in two-dimensional hole gas of black phosphorus. Nano Lett 2016;16:7768–73.
[93] Si MW, Yang LM, Du YC, et al. Black phosphorus field-effect transistor with record drain current exceeding 1 A/mm. 2017 75th Annual Device Research Conference (Drc), 2017.
[94] Ling ZP, Zhu JT, Liu X, et al. Interface engineering for the enhancement of carrier transport in black phosphorus transistor with ultra-thin high-k gate dielectric. Sci Rep 2016;6:26609.
[95] Liu X, Ang KW, Yu W, et al. Black phosphorus based field effect transistors with simultaneously achieved near ideal subthreshold swing and high hole mobility at room temperature. Sci Rep 2016;6:24920.
[96] Dickerson W, Tayari V, Fakih I, et al. Phosphorus oxide gate dielectric for black phosphorus field effect transistors. Appl Phys Lett 2018;112:173101.
[97] Ahmed F, Kim YD, Choi MS, et al. High electric field carrier transport and power dissipation in multilayer black phosphorus field effect transistor with dielectric engineering. Adv Funct Mater 2017;27:1604025.
[98] Ryder CR, Wood JD, Wells SA, et al. Chemically tailoring semiconducting two-dimensional transition metal dichalcogenides and black phosphorus. ACS Nano 2016;10:3900–17.
[99] Huang Y, Qiao J, He K, et al. Interaction of black phosphorus with oxygen and water. Chem Mater 2016;28:8330–9.
[100] Tan SJR, Abdelwahab I, Chu L, et al. Quasi-monolayer black phosphorus with high mobility and air stability. Adv Mater 2018;30:1704619.
[101] Wan B, Zhou Q, Zhang J, et al. Enhanced stability of black phosphorus field-effect transistors via hydrogen treatment. Adv Electron Mater 2018;4:1700455.
[102] Wood JD, Wells SA, Jariwala D, et al. Effective passivation of exfoliated black phosphorus transistors against ambient degradation. Nano Lett 2014;14:6964–70.
[103] Kim JS, Liu Y, Zhu W, et al. Toward air-stable multilayer phosphorene thin-films and transistors. Sci Rep 2015;5:8989.
[104] Gamage S, Fali A, Aghamiri N, et al. Reliable passivation of black phosphorus by thin hybrid coating. Nanotechnology 2017;28:265201.
[105] Jeong MH, Kwak DH, Ra HS, et al. Realizing long-term stability and thickness control of black phosphorus by ambient thermal treatment. ACS Appl Mater Interfaces 2018;10:19069–75.
[106] Jia J, Jang SK, Lai S, et al. Plasma-treated thickness-controlled two-dimensional black phosphorus and its electronic transport properties. ACS Nano 2015;9:8729–36.
[107] Kwak DH, Ra HS, Yang J, et al. Recovery mechanism of degraded black phosphorus field-effect transistors by 1,2-ethanedithiol chemistry and extended device stability. Small 2018. UNSP 1703194.

Hao Huang is currently a Ph.D. student under the direction of Prof. Lei Liao in School of Physics and Technology, Wuhan University. He received his B.E. degree in Microelectronics Science and Engineering from Wuhan University in 2016. His research interests focus on the high performance nanoelectronics.

Xuming Zou received his B.S. and Ph.D. degrees from Wuhan University in 2006 and 2016, respectively. He is currently an associate professor in School of Physics and Electronics, Hunan University since 2016. His research interests focus on high-performance optoelectronic devices based on 2D materials.

Xingzhong Zhao is currently a professor at Department of Physics, Wuhan University. He received B.S. degree in Wuhan University in 1982, M.S. degree in Wuhan University supervised by Prof. Ren-Hui Wang in 1985, and Ph.D. degree in Beijing University of Science and Technology under Prof. Jun Ke's direction in 1989. As postdoctor researcher at Materials Research Institute in Pennsylvania State University, supervised by National Academy of Engineering members Prof.Rustum Roy and Prof.L.E.Cross. His research interests are mainly about dye-sensitized solar cells (DSSCs), microfluidic systems & nanostructure devices and pizeoelectric materials.

Lei Liao is currently a professor at School of Physics and Electronics, Hunan University, where he received his B. S. and Ph.D. degrees, both in Physics. From 2009 to 2011, he worked as a postdoctoral researcher in Prof. Xiangfeng Duan's group at the Department of Chemistry and Biochemistry, University of California, Los Angeles, and then he worked as a professor at Department of Physics, Wuhan University from 2011 to 2016. His research focuses on the high performance thin film transistor based on nanomaterials.